This is an *Accepted Manuscript*, which has been through the Royal Society of Chemistry peer review process and has been accepted for publication.

Accepted Manuscripts are published online shortly after acceptance, before technical editing, formatting and proof reading. Using this free service, authors can make their results available to the community, in citable form, before we publish the edited article. We will replace this *Accepted Manuscript* with the edited and formatted *Advance Article* as soon as it is available.

You can find more information about *Accepted Manuscripts* in the **Information for Authors**.

Please note that technical editing may introduce minor changes to the text and/or graphics, which may alter content. The journal's standard **Terms & Conditions** and the **Ethical guidelines** still apply. In no event shall the Royal Society of Chemistry be held responsible for any errors or omissions in this *Accepted Manuscript* or any consequences arising from the use of any information it contains.

Experimental and Theoretical Studies of Structural Phase Transition in Novel Polar Perovskite-like [C$_2$H$_5$NH$_3$][Na$_{0.5}$Fe$_{0.5}$(HCOO)$_3$] Formate

Maciej Ptak,*,[a] Mirosław Mączka,[a] Anna Gągor,[a] Adam Sieradzki,[b] Alessandro Stroppa,[c] D. Di Sante,[c,d] Juan Manuel Perez-Mato,[e] and Lucyna Macalik[a]

ABSTRACT

We report the synthesis, single crystal x-ray diffraction, thermal, dielectric, Raman and infrared studies of novel heterometallic formate [C$_2$H$_5$NH$_3$][Na$_{0.5}$Fe$_{0.5}$(HCOO)$_3$] (EtANaFe). The thermal studies show that EtANaFe undergoes a second-order phase transition at about 360 K. X-ray diffraction data revealed that the high-temperature structure is monoclinic, space group $P2_1/n$, with dynamically disordered ethylammonium (EtA$^+$) cations. EtANaFe possesses polar low-temperature structure with the space group Pn, and in principle, is ferroelectric below 360 K. Dielectric data show that the reciprocal of the real part of dielectric permittivity above and below phase transition temperature follows the Curie-Weiss, as expected for a ferroelectric phase transition. Based on theoretical calculations, we estimated polarization as (0.2, 0, 0.8) μC/cm^2, i.e., lying within the *ac* plane. The obtained data also indicate that the driving force of the phase

transition is ordering of EtA^+ cations. However, this ordering is accompanied by significant distortion of the metal formate framework.

Introduction

Inorganic compounds crystallizing in a perovskite architecture have been extensively studied due to their wide range of interesting and useful properties. For instance, some perovskite manganites exhibit colossal magnetoresistance and many perovskite oxides exhibit ferroelectric properties.[1,2] Another family of widely studied compounds crystallizing in the perovskite architecture are hybrid organic-inorganic compounds of general formula ABX_3 with A= protonated amine, B= Pb, Sn, and X= Cl, Br, I.[3,4] These compounds have been recognized as very attractive materials for ferroelectric photovoltaic devices.[3,4] The third interesting family of compounds crystallizing in the perovskite architecture are alkylammonium metal formates. These compounds have been very extensively studied in recent years due to the magnetic, ferroelectric, gas sorption and multiferroic properties.[5-15] Most of the studies were devoted to $[cat][M(HCOO)_3]$ formates with divalent cations such as M=Mg, Zn, Mn, Fe, Co, Ni, Cu.[5-13] However, very recently a group of heterometallic perovskite formates with a general formula $[cat][M^I_{0.5}M^{III}_{0.5}(HCOO)_3]$ was discovered but up to now only two compounds belonging to this family are known, i.e. $[DMA][Na^I_{0.5}Fe^{III}_{0.5}(HCOO)_3]$ (DMANaFe) and $[DMA][Na^I_{0.5}Cr^{III}_{0.5}(HCOO)_3]$ (DMANaCr, where DMA = dimethylammonium cation).[14,15] These compounds can be regarded as obtained from the $[DMA][M(HCOO)_3]$ perovskites by replacing divalent metal cations by sodium and trivalent cations.[14]

Extensive studies on $[cat][M(HCOO)_3]$ formates showed that the size of the organic cation and its bonding strength to the anionic metal formate framework plays very important role in stability of the

structure and decides on properties of the obtained compounds.[5-13,16] For instance, [DMA][M(HCOO)$_3$] formates crystallizing in the trigonal space group $R\bar{3}c$ with the disordered DMA$^+$ cations located in the cages of the network exhibit order-disorder phase transition into ferroelectric structure at 160-279 K.[5,6,11] On the other hand, [C$_2$H$_5$NH$_3$][M(HCOO)$_3$] formates (M=Mg, Mn) crystallize in the non-centrosymmetric space group $Pna2_1$ with ordered EtA$^+$ cations.[10,16] It has been reported, however, that upon heating two phase transitions occur in [C$_2$H$_5$NH$_3$][Mg(HCOO)$_3$] at 374 and 426 K into trigonal and orthorhombic phase, respectively, with disordered EtA$^+$ cations.[10] It is also worth adding that the room temperature phases of [C$_2$H$_5$NH$_3$][M(HCOO)$_3$] formates (M=Mg, Mn) were predicted to exhibit ferroelectric properties.[9,10] We expect that also in case of [cat][M$^I_{0.5}$M$^{III}_{0.5}$(HCOO)$_3$] heterometallic formates the use of various organic cations should allow obtaining compounds possessing different structures and physicochemical properties.

Herein, we report synthesis and characterization of a novel heterometallic perovskite [C$_2$H$_5$NH$_3$][Na$^I_{0.5}$Fe$^{III}_{0.5}$(HCOO)$_3$] with EtA$^+$ cation in the cavity of the framework. We will show that this compound exhibits very interesting properties. In particular, it undergoes an order-disorder phase transition into a polar structure below 360 K.

Experimental

Materials and instrumentation

Heat capacity was measured using Mettler Toledo DSC-1 calorimeter with high resolution of 0.4 μW. Nitrogen was used as a purging gas. Weight of EtANaFe sample was 38.5 mg. The heating and cooling rate was 5 K/min. The excess heat capacity associated with the phase transition in EtANaFe was evaluated by subtraction from the data the baseline representing variation in the absence of the phase transitions. Ambient pressure dielectric measurements of examined sample

were carried out using a Novocontrol analyzer. Since the obtained single crystals were not big

enough to perform single crystal dielectric measurements, pellets made of well-dried samples

were measured instead. The pellets were placed between two copper, flat electrodes (diameter

6mm) of the capacitor with a gap of 0.3 mm. The small signal of an amplitude 1V was applied

across the sample. The temperature was controlled by the Novo-Control Quattro system, with use

of a nitrogen gas cryostat. The measurements were taken every 1 deg over the temperature range

from 300 to 400 K. Temperature stability of the samples was better than 0.1 K. Temperature-

dependent IR spectra in the 5-299 K range were measured for the sample in KBr pellet with the

Biorad 575C FT-IR spectrometer using a helium-flow Oxford cryostat. IR spectra in the 296-400

K range were measured using a home made furnace. The resolution was 2 cm^{-1}. Temperature-

dependent Raman spectra in the 50-3500 cm^{-1} range were measured using a Renishaw InVia

Raman spectrometer equipped with confocal DM 2500 Leica optical microscope, a

thermoelectrically cooled CCD as a detector, an argon laser operating at 488 nm and an edge

filter. Additional Raman spectra in the 20-400 cm^{-1} range were measured using the same

spectrometer but a diode laser operating at 830 nm as an excitation source and an Eclipse filter.

The sample for Raman measurements was placed in a cryostat cell THMS600.

Synthesis

$FeCl_2$ (98%, Aldrich), $C_2H_5NH_2 \cdot HCl$ (98%, Aldrich), N-ethylformamide (99%, Fluka), HCOOH

(98%, Fluka) and HCOONa (99%, Fluka) were commercially available and used without further

purification. Elemental analysis (C, H, N) was performed on a Elementar Vario EL CHNS

analyzer. The content of metal elements was determined by inductively coupled plasma method

(ICP), which was performed on a ARL 3410 ICP instrument. All crystals were prepared under

solvothermal conditions at 140 °C. In a typical experiment, a mixture of $FeCl_2$ (2 mmol),

ethylamine hydrochloride (2 mmol), HCOONa (6 mmol), N-ethylformamide (25 mL), H_2O (20 mL) and HCOOH (0.5 cm^3) was heated in a Teflon-lined microwave autoclave for 24 hours. Block light-yellow crystals were obtained by evaporating the solution at room temperature for 1 week. The crystals were filtered from the mother liquid and washed by ethanol. The yield was about 35 % based on the starting metal salts. Anal. Calcd for EtANaFe (%): C, 27.24; H, 4.99; N, 6.35; Fe, 12.66; Na, 5.21; Found (%): C, 27.17; H, 5.06; N, 6.27. ICP: Fe, 12.74; Na, 5.32. Ratio of Fe:Na=1:1.01. The phase purity of bulk sample was confirmed by a good match of its powder XRD pattern with the simulated one based on the single crystal structure (Figure S1, Supporting Information).

Crystallographic structure determination

Crystal structure was determined by means of the single-crystal X-ray diffraction performed on a KUMA KM4-CCD diffractometer operating in κ geometry and equipped with a two-dimensional CCD detector. The graphite monochromated Mo $K\alpha$ radiation was used. Data were collected at 297 and 377K in ω-scan mode with Δω=1.0^o using CrysAlisPro program.[17] An empirical absorption correction was applied using spherical harmonics implemented in SCALE3 ABSPACK scaling algorithm. The structure was solved by direct methods and refined by the full-matrix least-squares method by means of SHELXL-2014/7 program package.[18] All non-hydrogen atoms were refined anisotropically. Hydrogen atoms were refined with $U_{iso}(H)=1.2 \times U_{eq}$ of the corresponding parent atom, at 377 K restrains on N-C distances in disordered EtA$^+$ cations were introduced in order to maintain realistic bond lengths.

In addition, powder XRD pattern was obtained for all samples on an X'Pert PRO X-ray diffraction system equipped with PIXcel ultra-fast line detector, focusing mirror and Soller slits for $CuK\alpha_1$ radiation (λ=1.54056 Å).

Density Functional Calculations

In order to investigate the ferroelectric properties we performed density functional (DFT) calculations. The calculations have been carried out using the Vienna Ab initio Simulation Package (VASP),[19,20] using the projector augmented-wave (PAW) method with the PBEsol functional.[20] The energy cutoff was set to 400 eV and a 4x4x3 Monkhorst-Pack grid of k-points was used. The Berry phase approach was employed to calculate the ferroelectric polarization.[21]

Results and discussion

Thermal Properties

The DSC measurements show a heat anomaly at 360.6 K upon warming and 358.8 K upon cooling (Figure S2). Figure 1 shows that the calculated from the DSC data excess heat capacity associated with the phase transition (ΔC_p peak) is strongly asymmetric. The change in entropy at the phase transition is not sharp but ΔS decreases gradually with decreasing temperature from about 360 K to about 250 K (Figure 1). Such temperature dependence of ΔC_p and ΔS suggests that the phase transition has a second-order character.

The associated change in enthalpy ΔH and entropy ΔS was estimated to be ~0.86 KJmol^{-1} and ~2.5 Jmol^{-1}K^{-1}, respectively. These values are almost an order of magnitude smaller than those reported for $[C_2H_5NH_3][Mg(HCOO)_3]$ (ΔH~5.3 KJmol^{-1} and ΔS~14 Jmol^{-1}K^{-1} for the phase transition at 374 K, and ΔH~7.0 KJmol^{-1} and ΔS~17 Jmol^{-1}K^{-1} for the phase transition at 426

K).[10] They are however comparable to those reported for many [cat][M(HCOO)$_3$] compounds with DMA$^+$ or formamidinium cations.[5,6,12] This result shows that the phase transition in EtANaFe has very different character when compared to the phase transitions observed in ethylammonium magnesium formate but may have similar character as in other mentioned above compounds. This conclusion is consistent with the observation of Shang *et al* that the phase transitions in ethylammonium magnesium formate are very violent and accompanied by large changes in the metal formate framework whereas [cat][M(HCOO)$_3$] formates with other protonated amines show very different behavior, that is, the phase transitions in these compounds are associated with ordering of organic cations and small changes in the metal formate frameworks.[10]

It is worth adding that according to our X-ray diffraction studies, the EtA$^+$ cation shows disorder in the high temperature (HT) phase (see discussion in the next paragraphs of the present paper). For an order-disorder transition, $\Delta S = R\ln(N)$, where N is the number of sites for the disordered system. In our case N=2 and therefore ΔS should be 5.8 Jmol^{-1}K^{-1}. Our data show that the experimental ΔS is only half of the expected value. This result might indicate that the phase transition is more complex than expected on the basis of a simple order-disorder model.
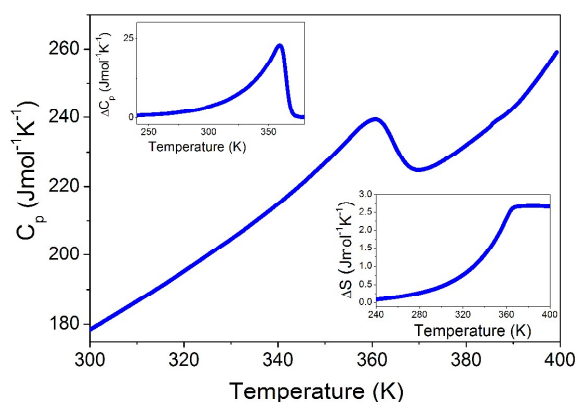
Figure 1. The heat capacity of EtANaFe measured in a heating mode. The insets show the change

in C_p and S related to the phase transition.

Dielectric properties

The overall temperature dependence of the real (ε') part of the dielectric permittivity is shown in

Figure 2. An anomalous relatively sharp peak is observed around 362 K, in good agreement with

the DSC data. This λ-type anomaly in the real part of the dielectric permittivity of a material may

imply a ferroelectric phase transition, although this should be directly verified *via* polarization

measurements. However, despite the lack of the dielectric hysteresis loop observation for this

compound, we can discern a few additional identities showing evidence of the character of the

phase transition. Thus, according to the ferroelectric theories, the reciprocal of real part of

dielectric permittivity above and below phase transition temperature follows the Curie-Weiss

law, $\varepsilon = C/(T - T_c)$, where C is the Curie constant and T_c is the Curie-Weiss temperature. These two

parameters may provide considerable information of the phase transition, including the transition

type (displacive or order/disorder) and the order of the transition (first or second order).

Therefore, this behavior was analyzed in order to obtain more understanding of the phase

transition type in this compound (Figure 2b). The magnitudes of the Curie constants are of about

10^3 in both phases, indicating the order-disorder nature of the observed transition. The ratio of

the Curie constants in the low- to high-temperature phases is equal to 1.6, which is close to 2 (the

phenomenological value for the second-order ferroelectric phase transition).[22] The dielectric loss

spectra additionally confirm the phase transition at about 360K (Figure 1c).
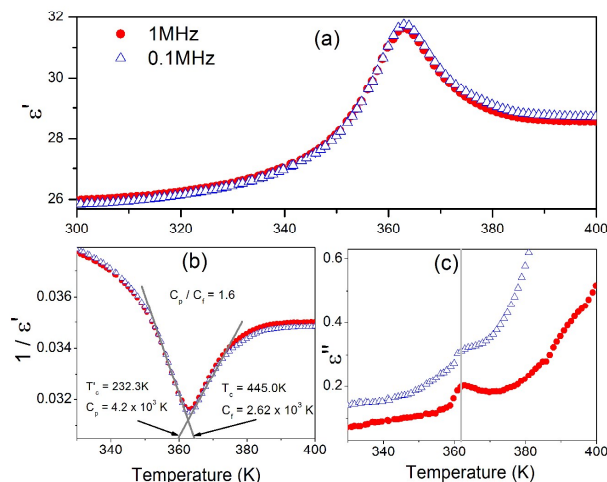
Figure 2. (a) Temperature dependence of the real part of the dielectric permittivity of EtANaFe at selected frequencies, (b) Curie–Weiss fittings of dielectric permittivity above and below the phase transition temperature at 0.1 MHz, and (c) the dielectric permittivity loss *vs* temperature.

Structural Studies

The details on data collection and reduction are given in Table 1. Table 2 summarizes the selected bonds lengths and angles. The detailed information about the crystal geometry is placed in supplementary materials, Table S1.

EtANaFe crystallizes in the monoclinic, polar space group *Pn* and transforms to centrosymmetric $P2_1/n$ space group at around 360 K. Metal ions are octahedraly coordinated. Each metal ion is connected to six metal neighbors through the six formate ligands in the anti-anti mode configuration. Na^+ and Fe^{3+} nodes are distributed alternately, thus each Na^+ ion connects to six Fe^{3+} ions and vice versa. The perovskite-like metal formate substructure is formed which accommodates EtA^+ template in the pseudo-cubic cavities. The cavity volume calculated with the PLATON program[23] is 75 $Å^3$ and 80 $Å^3$ in the room- and high-temperature

phase, respectively. Figure 3 illustrates the crystal packing of EtANaFe in both phases. The

crystal structure EtANaFe is a modification of the metal formate frameworks reported for

$[C(NH_2)_3][M^{II}(HCOO)_3]$ that crystallizes in the orthorhombic *Pnna* space group[24] with lattice

parameters similar to the metrics of EtANaFe. Introduction of large Na^+ ion (r_i=1.32 Å) leads to

deformation of the metal formate framework and reduction of the symmetry to the monoclinic.

The *P2₁/n* space group is a maximal subgroup of *Pnan* (in the standard setting *P2₁/c* is a maximal
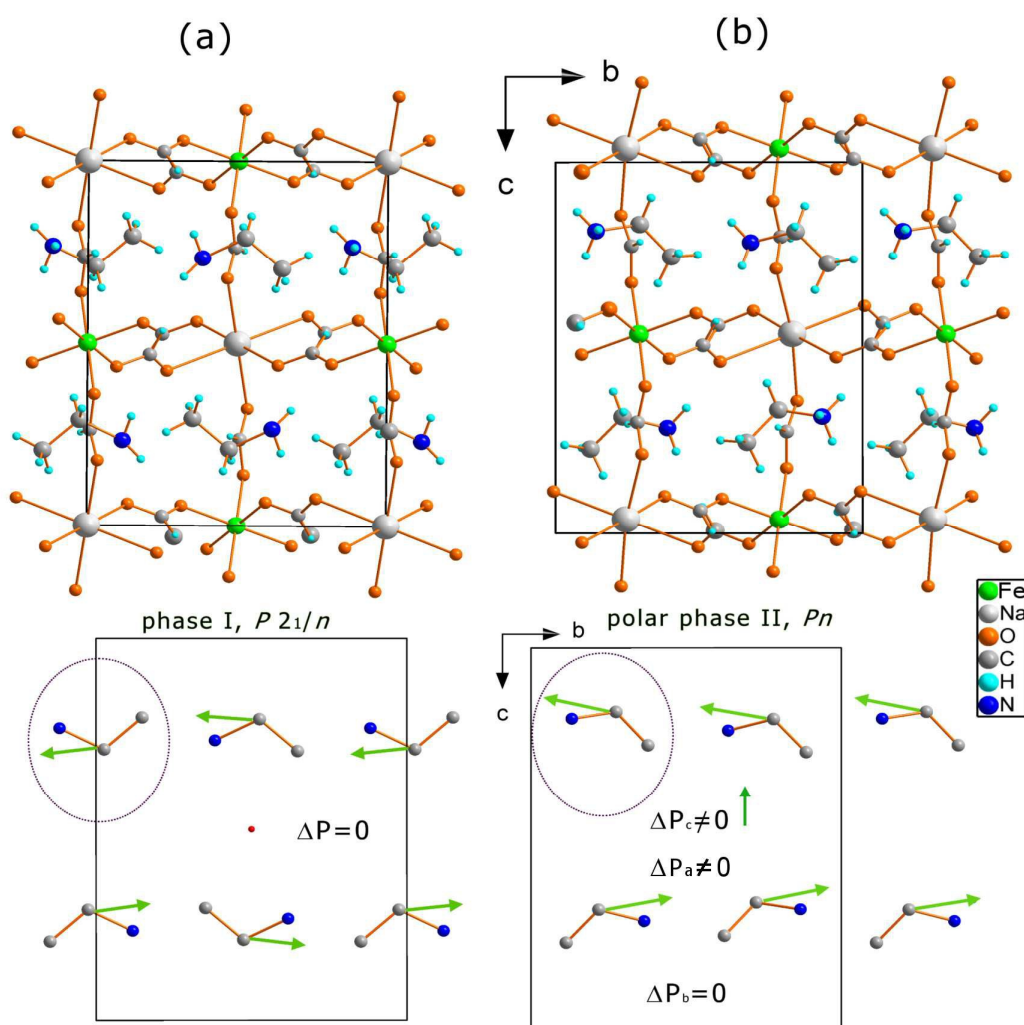
non-isomorphic subgroup of *Pnna*).[25]

Figure 3. Crystal structure packing of the EtANaFe, (a) high temperature, centrosymmetric phase I, T=377 K; (b) polar phase II, T=297 K. The pictures in the bottom present the cationic substructure, hydrogen atoms have been omitted for the picture clarity. Every EtA^+ has an internal dipole moment represented by the green arrow. The resultant dipole moment from all EtA^+ in phase I is equal to zero due to the presence of the symmetry center (red dot). In the polar phase II, non-compensated EtA^+ dipoles give rise to the spontaneous polarization that occurs perpendicularly to b direction. For the picture clarity one of the two possible orientations for EtA^+ in phase I has been drown.

In the high temperature phase I metal cations are located on the C_i symmetry sites. The EtA^+ counterions are dynamically disordered over two symmetrically independent positions. Each of them is occupied with ~50% probability; see Figures 4 and 5. The structural phase transition at T=360 K leads to the reduction of the symmetry form $P2_1/n$ to Pn. It manifests in distortion of the metal formate framework (all atoms occupy general positions with C_1 symmetry, Figure S3) and ordering of EtA^+ cations due to reduction of the size of the crystal voids and thermally induced motions.
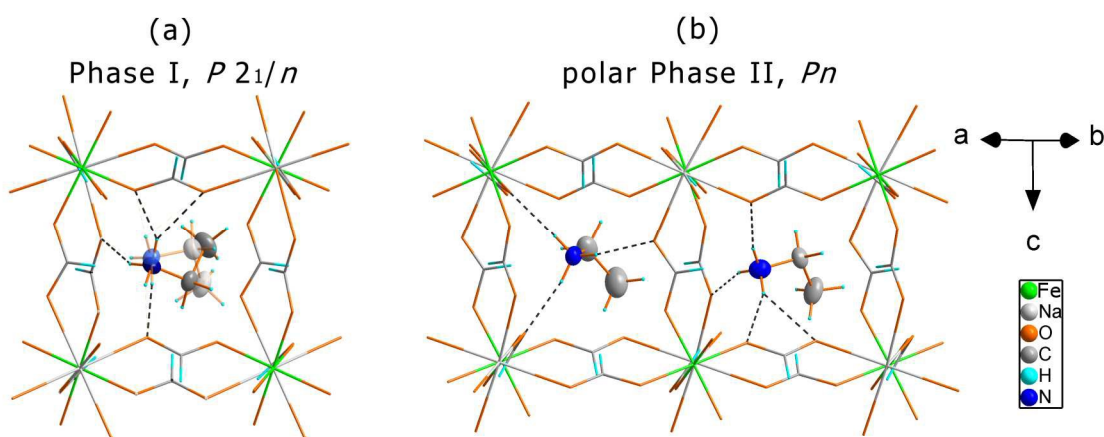
Figure 4. Spatial arrangement of the cations in the EtANaFe metal formate framework; (a) high temperature phase I, T=377K, (b) polar phase II, T=297K. The dotted lines represent N-H…O hydrogen bonds. Site occupation factor for disordered cations in Phase I is ~0.5 for each of the state.
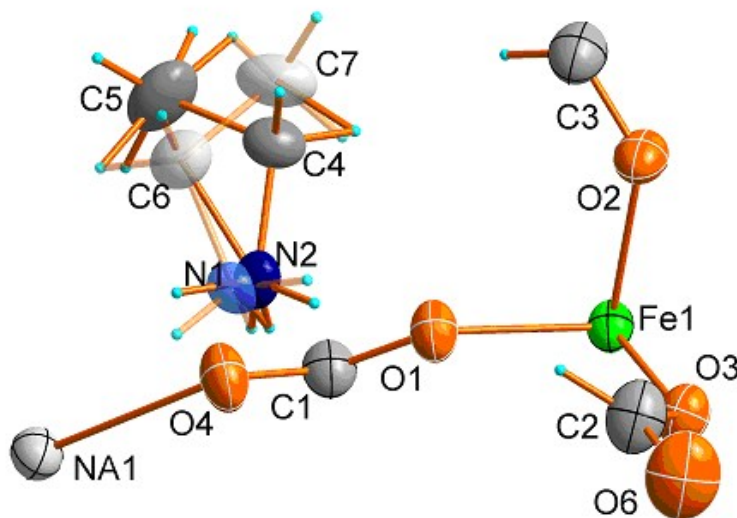

Figure 5. The content of the asymmetric unit in the high-temperature phase of EtANaFe formate, T=377 K. The EtA$^+$ is disordered over two symmetrically independent positions. Both are occupied with ~50% probability.

In phase II there are two non-equivalent EtA$^+$ counter ions in the asymmetric unit. They are ordered and form conventional N-H…O hydrogen bonds to the formate oxygen ions. The donor to acceptor distances, in N—H···O hydrogen bonds, range from 2.860(6) to 3.298(7) Å in the polar phase *Pn*. After the transition the length of hydrogen bonds changes insignificantly and range from 2.92(2) to 3.08(2) Å. The detailed information concerning the geometry of the hydrogen bonds is presented in the supplementary materials in Table S2.

Each EtA+ has an internal dipole moment. In phase I, due to the presence of the symmetry center the resultant dipole moment is equal to zero. In the *Pn* phase the spatial arrangement of the EtA+ dipole moments give rise to the spontaneous polarization within the (*a,c*) plane. The components of the dipole moments along the *b* axis are compensated due to the presence of the *n* glide plane, which is illustrated in Figure 3. The symmetry mode analysis performed in AMPLIMODES[26] revealed that significant contribution to the phase transition and thus to the appearance of the spontaneous polarization, have displacements of the Na^+, Fe^{3+} cations and formate linkers. The metal formate framework experiences significant structural distortion as a result of the phase transition. The structure of the low temperature phase II has two distortion modes; a primary one that yields *Pn* symmetry and secondary one that has the symmetry of the high temperature phase *P2₁/n*. The displacements of the metal ions have the symmetry of the primary mode and contribute to the spontaneous polarization. Each metal has almost the same contribution to the primary mode, equal to ~0.2 Å. The displacements of oxygen and carbon atoms from the positions that were occupied in phase I are also large. The maximum atomic displacement in the distortion concerns O(6) oxygen that shifts 0.3 Å. Not much smaller are the shifts of the remaining oxygen and carbon atoms which contribute significantly to the total distortion. They have the symmetry of both lattice modes with primary mode dominating. The total distortion amplitude that is given by the square root of the sum of the squares of all atomic displacements is equal to 1.3 Å. The details concerning the atomic displacements between the two phases are given in supplementary materials in Table S3. The analysis was done only for these atoms that are ordered in both phases, *it est.* metal centers, oxygen and carbon atoms from the formate linkers. The hydrogen atoms as well as the disordered over two positions in the *P2₁/n* phase EtA^+ cations were not included.

The distortion amplitude associated with the primary mode is equal to 1.3 Å, whereas the amplitude of the secondary mode is very weak, equal only to 0.14 Å, which is one order of magnitude smaller. Concerning the values of the distortion modes the system seems to be a 'well-behaved' ferroelectric, with atomic displacements of the order of 0.5 Å, as in classical ferroelectrics, and with very weak secondary modes.[26]

Table 1. Experimental details for EtANaFe at 297 and 377 K.

Chemical formula	$C_{10}H_{22}FeN_2NaO_{12}$	$C_{10}H_{22}FeN_2NaO_{12}$
M_r	441.13	441.13
Crystal system, space gr.	Monoclinic, Pn	Monoclinic, $P2_1/n$
Temperature (K)	297	377
a, b, c (Å)	8.1176 (1), 9.2906 (1), 12.0776 (1)	8.1102 (2), 9.3794 (4), 12.1341 (4)
β (°)	91.3953 (10)	91.125 (3)
V (Å^3)	910.59 (2)	922.85 (6)
z	2	2
μ (mm^{-1})	0.92	0.90
Crystal size (mm)	$0.15 \times 0.11 \times 0.10$	$0.15 \times 0.11 \times 0.10$
T_{min}, T_{max}	0.878, 1.000	0.976, 1.000
measured, independent, observed [I > 2σ(I)] ref.	13093, 3442, 2987	3623, 1737, 1519
R_{int}	0.040	0.021
(sin θ/λ)$_{max}$ (Å^{-1})	0.609	0.610

14

$R[F^2 > 2\sigma(F^2)]$, $wR(F^2)$, S   0.036, 0.072, 1.03   0.043, 0.099, 1.20

No. of reflections	3442	1737

No. of parameters	240	150

No. of restraints	2	42

$\Delta\rho_{max}$, $\Delta\rho_{min}$ (e $Å^{-3}$)   0.24, -0.28   0.21, -0.23

Absolute   structure 0.42 (2)   –
parameter (^{a})

Table 2. Selected bond lengths (Å) and angles (°).

	EtANaFe at 297K	EtANaFe at 377K
Fe—O	1.999(4)-2.021(3)	2.006(2)-2.015(2)
Na—O	2.384(5)-2.515(4)	2.412(3)-2.532(2)
O—C	1.206(7)-1.281(6)	1.213(4)-1.275(4)
N—C	1.460(8)-1.475(8)	1.460(1)
C7—C8	1.446(10)	1.499(1)
Cis O-Fe-O	88.2(2)-92.4(2)	89.08(8)-90.92(8)
Trans O-Fe-O	178.1(2)-179.5(2)	180
Cis O-Na-O	84.3(2)-94.5(2)	87.21(9)-92.79(9)
Trans O-Na-O	172.4(2)-179.2(2)	180
O-C-O	123.7(5)-127.4(5)	124.7(3)-127.6(3)

DFT calculations

Starting from the low symmetry structure, we introduced a reference non-polar structure which

mimics a displacive type phase transition between the paraelectric and ferroelectric structure. In

our calculations the reference structure is assumed to be fully ordered and centric. Although the

real nature of the phase transition must be ascribed to order-disorder type, this approach is useful

for evaluating the ferroelectric polarization using ab-initio methods. The low symmetry structure

can be obtained from the reference structure by small atomic displacements. In this case, the low

symmetry structure is said to be pseudosymmetric to the high symmetry (reference) structure. It

is important to note that the reference structure is only a computational tool for evaluating the

polarization and, in general, it does not need to be a 'real' paraelectric structure. For instance, it

may be used   instead of a real disordered paraelectric structure, which would be difficult to

simulate. From a physical point of view, the approach is well justified since the estimated

polarization does not depend on the choice of the reference paraelectric structure. Furthermore,

by considering an ordered centric structure instead of a disordered one, one can use distortion

mode analysis in order to analyze the displacement leading to the polar structure (symmetry

mode analysis).[27-31] In our case, the reference non-polar structure has $P2_1/n$ symmetry. We

impose the AFM-A type ordering on Fe atoms, i.e. Fe atoms are ferromagnetically coupled in-

plane but antiferromagnetically coupled between parallel planes along the c-axis. Figure 6 shows

the ferroelectric polarization as a function of λ, where λ is normalized amplitude of the atomic

distortion connecting the reference paraelectric structure to the ferroelectric one. We estimated

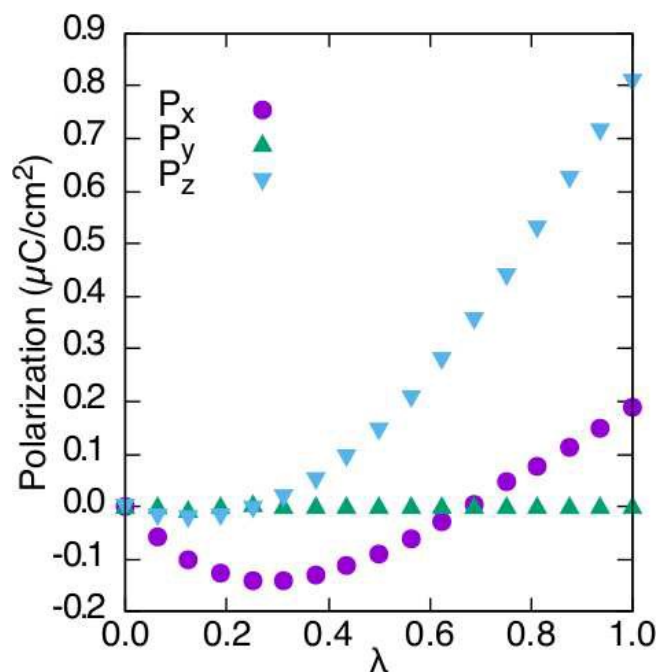polarization as $(0.2,0,0.8)$ $\mu C/cm^2$, i.e. lying the ac plane (Figure 6).

16

Figure 6. Ferroelectric polarization as a function of λ.

Vibrational Studies

Raman and IR spectra of the studied compound may be understood by dividing vibrations into internal vibrations of the EtA$^+$ and formate ions, and the lattice vibrations. Free HCOO$^-$ ion has C_{2v} symmetry, and its internal vibrations consist of the C-H stretching mode ν_1, the symmetric C-O stretching mode ν_2, the antisymmetric C-O stretching mode ν_4, the symmetric O-C-O bending (scissor) mode ν_3, the C-H in-plane bending mode ν_5, and the C-H out-of-plane bending mode ν_6.[11] Free EtA$^+$ cation has C_s symmetry and the 27 internal modes are distributed among the irreducible representation: $\Gamma = 16A'+11A''$.[32] These modes can be subdivided into symmetric stretching ($\nu_s(CH_2)$), antisymmetric stretching (($\nu_{as}(CH_2)$), scissoring ($\delta(CH_2)$), rocking ($\rho(CH_2)$), wagging ($\omega(CH_2)$) and torsion or twisting ($\tau(CH_2)$) modes of the CH_2 group as well as

symmetric stretching (ν_s), antisymmetric stretching (ν_{as}), bending (δ), rocking (ρ) and torsion (τ) modes of the CH_3 and NH_3 groups. The remaining three vibrations correspond to symmetric stretching (ν_s(CCN)), antisymmetric stretching (ν_{as}(CCN)) and bending (δ(CCN)) modes of the CCN skeleton. The lattice modes may be divided into translational (T') modes of sodium, iron, formate and EtA$^+$ ions as well as librational (L) modes of formate and EtA$^+$ ions.

The Raman and IR spectra of the studied compounds are presented in Figures 7-9, S4 and S5. The observed IR and Raman frequencies (in cm^{-1}) are listed in Table S4 together with suggested assignments that were mostly based on literature data.[11,12,14,15,32-35] The assignment of bands corresponding to internal vibrations of the HCOO$^-$ ions could easily be done by comparison with the spectra of studied recently DMANaFe.[14] Internal modes of EtA$^+$ cation can also be easily identified based on DFT calculations performed for isolated EtA$^+$ cation and experimental studies of [$C_2H_5NH_3$]$_2$SiF$_6$ and ethylammonium chloride.[32-34] Assignments of lattice modes is more difficult since these modes may be strongly coupled. Nevertheless, our former studies of related formates showed that translational and librational modes of DMA$^+$ cation contributed to the modes observed below 170 cm^{-1}.[11] Prasad assigned the Raman bands of ethylammonium chloride in the 119-192 cm^{-1} to L(EtA) modes.[34] Our spectra show presence of strong Raman bands at 117-171 cm^{-1} and weaker bands below 100 cm^{-1}. Since former studies of related formates indicated that the most intense Raman bands correspond mainly to L(HCOO) modes,[11,12,14,15,35] we attribute the 117-171 cm^{-1} bands to librations of formate ions and those below 100 cm^{-1} to motions of ethylammonium cations. The remaining modes in the 210-340 cm^{-1} range can be attributed to translations of formate, sodium and iron ions, similarly as discussed for DMANaFe.[14]
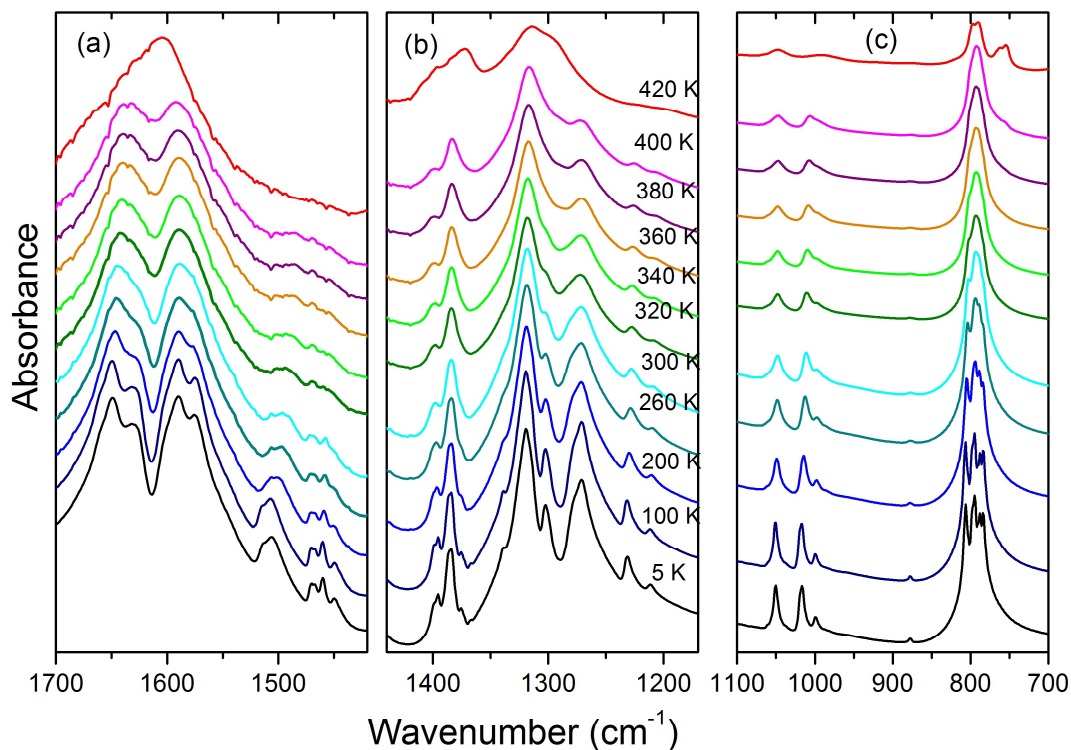
Figure 7. Details of the IR spectra corresponding to the spectral ranges (a) 1420-1700, (b) 1170-1440 and (c) 700-1100 cm^{-1} for EtANaFe. The spectrum measured at 420 K upon heating shows presence of bands near 760 cm^{-1}, disappearance of splitting near 1600 cm^{-1} and disappearance of bands in the 1430-1510 cm^{-1} region. These changes indicate decomposition of the sample associated with lost of ethylamine molecules.
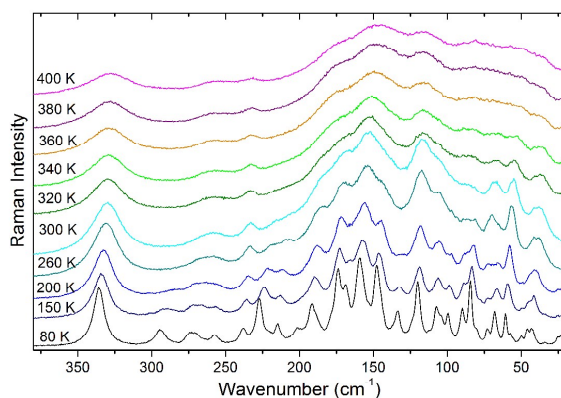
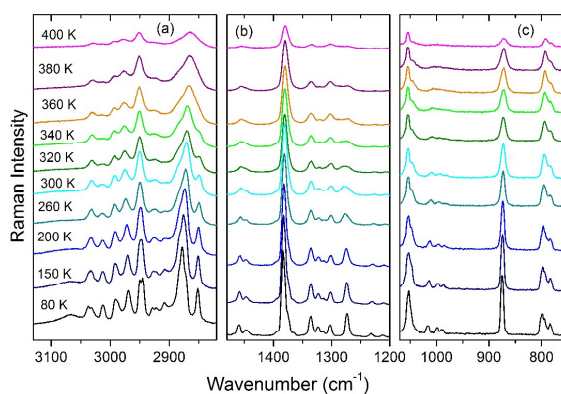Figure 8. Temperature-dependent Raman spectra of EtANaFe in the 22-380 cm^{-1} range.

Figure 9. Details of the Raman spectra corresponding to the spectral ranges (a) 2820-3130, (b) 1200-1480 and (c) 760-1070 cm^{-1} for EtANaFe.

Temperature-dependent Raman and IR studies

Temperature-dependent IR studies show that upon cooling from 400 K, internal bands of HCOO^{-} ions exhibit relatively weak narrowing. However, some of these bands split below T_c and many new bands appear. For instance, the 793 cm^{-1} IR band at 380 K splits into 797 and 795 cm^{-1} components and two new bands appear at 788 and 784 cm^{-1} when temperature decreases to 5 K.

Similar behavior is also observed for the Raman bands. For instance, the 793 cm^{-1} Raman band splits into 802, 798 and 794 cm^{-1} bands at 80 K (see Table S5). The observed splitting and appearance of new bands indicates distortion of the metal formate framework, and this observation is consistent with x-ray diffraction data that revealed decrease of symmetry from $P2_1/n$ to Pn and increase of unique $HCOO^-$ ions from 3 in the high-temperature phase to 6 in the low-temperature phase. It is worth noting that the observed splitting is not abrupt at the phase transition temperature but rather continuous. This behavior is consistent with the second-order character of the phase transition.

In contrast to weak narrowing of the bands corresponding to internal vibrations of the formate ions, the bands corresponding to internal vibrations of EtA^+ cation exhibit very pronounced narrowing. For instance, only one very broad Raman band is observed at 400 K at about 999 cm^{-1} (its full width at half maximum, FWHM, is 35.1 cm^{-1}) but three bands at 1017, 99 and 988 cm^{-1} upon cooling to 80 K with FWHM value of 7.8, 5.9 and 8.2 cm^{-1}, respectively. These bands correspond to the $\rho(NH_3)$ mode and our previous studies of related formates with DMA^+ cation showed that rocking modes of amine group are especially sensitive to order-disorder phenomena in these MOFs.[11,12,14,36] It is interesting to notice that rocking modes of the CH_2 and CH_3 groups, observed in the 1200-1280 cm^{-1} range, also exhibit pronounced narrowing upon cooling (Figures 7 and 9). The observed temperature-dependence of the discussed modes indicates that the phase transition in this compound is mainly due to ordering of EtA^+ cations, which are dynamically disordered in the high-temperature phase. This orientational disorder leads to broadening of vibrational bands and when dynamic disorder prevails over the phonon decay process, FWHM of a band can be expressed by:

$$FWHM = A + BT + C\exp(-E_a/kT), \qquad (1)$$

where E_a is the activation energy, k is the Boltzmann constant and T is the temperature.[37] The linear term corresponds to anharmonic effects and the exponential one described thermally activated reorientational processes. Figure 10 shows temperature-dependence of FWHM for the $\rho(NH_2)$ IR-active mode observed at 1007 cm^{-1} at 400 K. Fitting of the experimental data with the eq. (1) gives A=6.6 cm^{-1}, B=0.005 cm^{-1}K^{-1}, and E_a=166 meV. The value of E_a is larger than the 92 and 135 meV values found for the studied by us previously $[(CH_3)_2NH_2][Mn(HCOO)_3]$ and $[NH_2\text{-}CH^+\text{-}NH_2][Mn(HCOO)_3]$ compounds.[11,12] Note that the reorientational processes to the observed broadening are negligible below 200 K (Figure 10), indicating that the ordering of EtA$^+$ ions is nearly complete below this temperature. Order-disorder character of the phase transition is further confirmed by very pronounced narrowing of the lattice modes (Figure 8), which are very sensitive to changes in the long-range order.

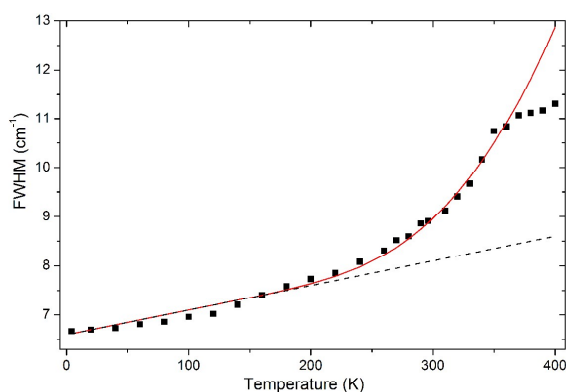
Figure 10. Temperature dependence of FWHM of the 1007 cm^{-1} IR band corresponding to the $\rho(NH_2)$ mode (squares). Solid red line shows fit on the data to eq. 1. The black dash line represents contribution due to reorientational processes.

Effect of alkylammonium cation of structural distortion and the phase transition mechanism

The obtained data show that the high-temperature structures of EtANaFe and studied by us previously DMANaFe,[14] have similar frameworks composed of NaO_6 and FeO_6 octahedra connected by formate ligands. They also have disordered EtA^+ and DMA^+ cations, which form hydrogen bonding with the anionic frameworks. We showed that in the DMANaFe the H-bonds formed between the NH_2 groups and oxygen atoms of the NaO_6 octahedra are stronger (N···O distances are 2.8852 and 3.0769 Å) than the H-bonds formed between the NH_2 groups and oxygen atoms of the FeO_6 octahedra (N···O distances are 3.5321 and 3.0957 Å).[14] Similar effect is also observed for EtANaFe. Namely, each of the disordered EtA^+ molecules form only one H-bond to the O3 atom of FeO_6 with the N···O distances of 2.91 and 3.14 Å, whereas three bonds are formed to the O4, O5 and O6 atoms of NaO_6 with the N···O distances ranging from 2.79 to 3.26 Å (Table S2). It is worth noting that stronger H-bond network to the NaO_6 ocathedra is revealed not only by very short N···O distance (2.79 Å) but also by formation of three H-bonds between each EtA^+ cation and the NaO_6 groups, when compared to only one such bond between each EtA^+ cation and the FeO_6 groups. The strongly asymmetric pattern of H-bonds in EtANaFe is different from that in DMANaFe, where each DMA^+ cation formed two H-bonds with NaO_6 and FeO_6. This difference is responsible for different distortion of the anionic framework. Distortion of the MO_6 octahedra can be quantified by calculating the distortion parameter Σ:

$$\Sigma = \sum_{i=1}^{12} \left(\left| \varphi_i - 90 \right| \right)$$

(2)

where φ_i denote 12 *cis* O-M-O angles in the coordination sphere.[38] The distortion parameters Σ are 10.54° and 6.96° for FeO_6 and NaO_6 in the room-temperature structure of DMANaFe, and 9.24° and 23.8° for FeO_6 and NaO_6 in the high-temperature phase of EtANaFe. As can be noticed, distortion parameters Σ of FeO_6 are similar in DMANaFe and EtANaFe but this parameter is much larger for NaO_6 in EtANaFe.

Both DMANaFe and EtANaFe undergo structural phase transitions, which are associated with ordering of organic cations and distortion of the anionic framework. However, in DMANaFe the high- and low-temperature phases are centrosymmetric, with R-3 and P-1 symmetry,[14] wherease for EtANaFe symmetry changes from centrosymmetric $P2_1/n$ to polar *Pn*. Furthermore, the phase transition temperature is much higher for EtANaFe (360 K) than DMANaFe (167 K).[14] Shift of T_c towards higher value when DMA^+ cations are replaced by EtA^+ ones can be attributed to more robust H-bond network due to presence of three H atoms in the NH_3 group of EtA^+ cation and only two H atoms in the NH_2 group of DMA^+. The calculated distortion parameters Σ are 67.21° and 62.07° for FeO_6 and NaO_6 in the low-temperature structure of DMANaFe (at 110 K), and 11.71° and 32.5° for FeO_6 and NaO_6 in the low-temperature phase of EtANaFe (at 297 K). This comparison shows that the phase transition in DMANaFe leads to very large distortion of the MO_6 octahedral units (Σ increases more than six times) but distortion of FeO_6 and NaO_6 is comparable. In case of EtANaFe, the phase transition leads to much smaller change in the distortion parameter (less than 37 %) but similarly as for DMANaFe, the change in Σ is comparable for NaO_6 and FeO_6.

CONCLUSIONS

We have synthesized novel heterometallic formate crystallizing in the perovskite-like architecture, EtANaFe. DSC data revealed that this compound undergoes a structural phase transition at about 360 K. X-ray diffraction, Raman and IR measurements have demonstrated that EtA$^+$ cations are dynamically disordered in the high-temperature centrosymmetric monoclinic phase. Upon cooling, the hydrogen bond strength between the EtA$^+$ cations and anionic framework increases and at 360 K a structural transition occurs into a monoclinic phase with ordered EtA$^+$ cations. This low-temperature phase is polar, and in principle, ferroelectric. Dielectric data show that the Curie-Weiss law is fulfilled and values of the Curie-Weiss constants supports order-disorder mechanism of the phase transition. DFT calculations idicate that the low-temperature phase of EtANaFe may have ferroelectric properties with ferroelectric polarization located within the *ac* plane. IR and Raman data also show that EtA$^+$ ions retain some degree of orientational motions down to about 200 K. They also indicate that ordering of EtA$^+$ cations is associated with distortion of the metal formate framework.

It is worth adding here that room-temperature ferroelectric MOFs and molecular crystals are still scarce. It this respect, very promising molecular ferroelectric compounds discovered in recent years are monoclinic diisopropylammonium chloride and bromide with P_s=8.9 μC/cm^2 and 23 μC/cm^2, respectively. This very large polarization mainly comes from atomic displacement. The estimated by us electric plarization in EtANaFe is significantly lower (0.8 μC/cm^2) and ferroelectricity in this compound comes from ordering of EtA$^+$ cations.

Acknowledgements

Notes

[a]Institute of Low Temperature and Structure Research, Polish Academy of Sciences, Box 1410, 50-950 Wrocław 2, Poland; m.maczka@int.pan.wroc.pl; phone: +48-713954161; fax: +48-713441029

[b]Faculty of Fundamental Problems of Technology, Wrocław University of Technology, Wybrzeże Wyspiańskiego 27, 50-370, Wrocław, Poland

[c]CNR-SPIN, Via Vetoio, 67100 L'Aquila, Italy

[d]Department of Physical and Chemical Sciences, University of L'Aquila, Via Vetoio, Coppito (AQ), Italy

[e]Departamento de Fisica de la Materia Condensada, Facultad de Ciencia y Tecnologia, UPV/EHU, Bilbao, Spain

Electronic Supplementary Information (ESI) available: Figures S1-S6: X-ray diffraction, DSC traces, the content of the asymmetric unit in the high- and low-temperature phases, IR and Raman spectra. Tables S1-S4: selected geometric parameters for the structure refinement, atomic displacements after the symmetry change from $P2_1/n$ to Pn, and Raman and IR frequencies together with proposed assignments.

References

1 A. P. Ramirez, *J. Phys. Condens. Matter* 1997, **9,** 8171-8199.

2 K. M. Rabe, C. H. Ahn, J.-M. Triscone, Physics of Ferroelectrics: A Modern Perspective, Springer-Verlag, Berlin Heidelberg 2007.

3 (a) F. Hao, C. C. Stoumpos, D. H. Cao, R. P. H. Chang, M. G. Kanatzidis, *Nature Photonics* 2014, **8,** 489-494. (b) P. V. Kamat, *J. Am. Chem. Soc.* 2014, **136,** 3713-3714.

4 (a) A. Stroppa, C. Quarti, F. De Angelis, S. Picozzi, *J. Phys. Chem. Lett.* 2015, **6,** 2223-2231. (b) A. Stroppa, D. Di Sante, P. Barone, M. Bokdam, G. Kresse, C. Franchini, M.-H. Whangbo, S. Picozzi, *Nature Commun*. 2014, **5,** 5900.

5 (a) P. Jain, N. S. Dalal, B. H. Toby, H. Kroto, A. K. Cheetham, *J. Am. Chem. Soc.* 2008, **130,** 10450-1451. (b) P. Jain, V. Ramachandran, R. J. Clark, H. D. Zhou, B. H. Toby, N. S. Dalal and H. W. Kroto, A. K. J. Cheetham, *J. Am. Chem. Soc*., 2009, **131**, 13625-13627. (c) M. Guo, H. L. Cai, R. G. Xiong, *Inorg. Chem. Commun*. 2010, **13,** 1590-1598.

6 B. Pato Dolán, M. Sánchez-Andújar, L. C. Gómez-Aguirre, S. Yáñez-Vilar, J. Lopez-Beceiro, C. Gracia-Fernandez, A. A. Haghighirad, F. Ritter, S. Castro-Garcia and M. A. Señaris-Rodriguez, *Phys. Chem. Chem. Phys*., 2012, **14**, 8498-8501.

7 (a) D. W. Fu, W. Zhang, H. L. Cai, Y. Zhang, J. Z. Ge, R. G. Xiong, S. D. Huang and T. Nakamura, *Angew. Chem. Int. Ed*., 2011, **50**, 11947-11951. (b) Y. Tian, A. Stroppa, Y. Chai, L. Yan, S. Wang, P. Barone, S. Picozzi and Y. Sun, *Sci. Rep.* 2014, **4,** 6062.

8 (a) B. Pato Dolán, L. C. Gómez-Aguirre, J. M. Bermúdes-García, M. Sánchez-Andújar, A. Fondado, J. Mira, S. Castro-Garcia and M. A. Señaris-Rodriguez, *RSC Advances* 2013, **3,** 22404-22411. (b) A. Stroppa, P. Jain, P. Barone, M. Marsman, J. M. Perez Mato, A. K. Cheetham, H. W. Kroto and S. Picozzi, *Angew. Chem. Int. Ed*. 2011, **50,** 5847-5850.

9 D. Di Sante, A. Stroppa, P. Jain and S. Picozzi, *J. Am. Chem. Soc*. 2013, **135,** 18126-18130.

10 R. Shang, G. C. Xu, Z. M. Wang and S. Gao, *Chem. Eur. J*. 2014, **20,** 1146-1158.

11 (a) M. Mączka, A. Gągor, B. Macalik, A. Pikul, M. Ptak and J. Hanuza, *Inorg. Chem.*, 2014, **53**, 457-467. (b) M. Mączka, M. Ptak and L. Macalik, *Vib. Spectrosc.*, 2014, **71**, 98-104. (c) M. Mączka, W. Zierkiewicz, D. Michalska and J. Hanuza, *Spectrochim. Acta A.*, 2014, **128**, 674-680.

12 (a) M. Mączka, A. Ciupa, A. Gągor, A. Sieradzki, A. Pikul, B. Macalik and M. Drozd, *Inorg. Chem.*, 2014, **53**, 5260-5268. (b) A. Ciupa, M. Mączka, A. Gągor, A. Pikul, E. Kucharska, J. Hanuza, A. Sieradzki, A. *Polyhedron* 2015, **85,** 137-143.

13 A. Rossin, M. R. Chierotti, G. Giambiastiani, R. Gobetto and M. Peruzzini, *Cryst. Eng. Comm.*, 2012, **14**, 4454-4460.

14 M. Mączka, A. Pietraszko, L. Macalik, A. Sieradzki, J. Trzmiel and A. Pikul, *Dalton Trans.* 2014, **43,** 17075-17084.

15 M. Mączka, B. Bondzior, P. Dereń, A. Sieradzki, J. Trzmiel, A. Pietraszko and J. Hanuza, *Dalton Trans.*, 2015, **44,** 6871-6879.

16 Z. Wang, B. Zhang, T. Otsuka, K. Inoue, H. Kobayashi, M. Kurmoo, *Dalton Trans.* 2004, 2209-2016.

17 CrysAlisPro, Oxford Diffraction Ltd.,Version 1.171.34.44 (compiled Oct 25 2010,18:11:34).

18 G.M. Sheldrick, *Acta Cryst. A,* 2008, **64,** 112-122.

19 G. Kresse, J. Furthmüller, *Phys. Rev. B*. 1996, **54,** 11169–11186.

20 J.P. Perdew, A. Ruzsinszky, G. I. Csonka, O. A. Vydrov, G. E. Scuseria, I. A. Constantin, X. Zhou, K. Burke, *Phys. Rev. Lett.* 2008, **100,** 136406.

21 R. D. King-Smith, D.Vanderbilt, *Phys. Rev. B* 1993, **47,** 1651-1654.

22 B. A. Strukov, A. P. Levanyuk, *Ferroelectric phenomena in crystals, Springer-Verlag Berlin Heidelberg* 1998.

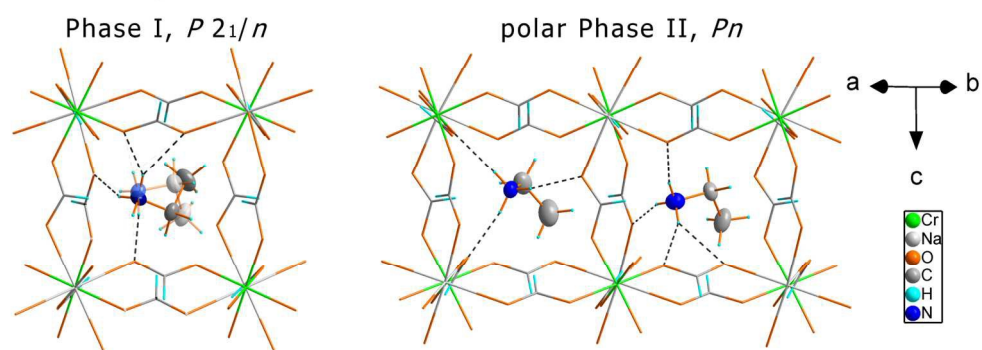23 PLATON, A Multipurpose Crystallographic Tool, A. L. Spek, Utrecht University, 2001.

24 K. L. Hu, M. Kurmoo, Z. Wang, S. Gao, *Chem. Eur. J.* 2009, **15,** 12050-12064.

25 International Tables for Crystallography, volume A; Kluwer Academic Publishers, Dordrecht/Boston/London 1995.

26 S. C. Abrahms, *Ferroelectrics* 1990, **104,** 37-50.

27 D. Orobengoa, C. Capillas, M. I. Aroyo, J. M. Perez-Mato, *J. Appl. Cryst. A* 2009, **42,** 820-833.

28 J. M. Perez-Mato, D. Orobengoa, M. I. Aroyo, *Acta. Cryst. A* 2010, **66,** 558-590.

29 E. Kroumova, M. I. Aroyo, J. M. Perez-Mato, S. Ivantchev, J. M. Igartua, H. Wondratschek, *J. Appl. Cryst.* 2001, **34,** 783-784.

30 C. Capillas, M. I. Aroyo, J. M. Perez-Mato, *Z. Krist.* 2005, **220,** 691-699.

31 C.Capillas, E. S. Tasci, G. de la Flor, D. Orobengoa, J. M. Perez-Mato, M. I. Aroyo, *Z. Krist.* 2001, **226,** 186-196.

32 D. Zeroka, J. O. Jensen, A. C. Samuels, *J. Mol. Struct.* 1999, **465,** 119-139.

33 A. Ouasri, A. Rhandour, M.-C. Dhamelincourt, P. Dhamelincourt, A. Mazzah, *Spectrochim. Acta A* 2003, **59,** 357-362.

34 P. S. R. Prasad, *J. Phys. Chem.* 1996, **100,** 888-890.

35 (a) M. Maczka, A. Pietraszko, B. Macalik, K. Hermanowicz, *Inorg. Chem.* 2014, **53,** 787-794. (b) M. Mączka, P. Kadłubański, P. T. C. Freire, B. Macalik, W. Paraguassu, K. Hermanowicz, J. Hanuza, *Inorg. Chem.* 2014, **53,** 9615-9624. (c) M.Maczka, K. Szymborska-Małek, A. Ciupa, J. Hanuza, J. *Vib. Spectrosc.* 2015, *77,* 17-24. (d) M. Mączka, T. A. Da Silva, W. Paraguassu, M. Ptak and K. Hermanowicz, *Inorg. Chem.* 2014, **53,** 12650-12657.

36 (a) A. Ciupa, M. Mączka, A. Gągor, A. Sieradzki, J. Trzmiel, A. Pikul and M. Ptak, *Dalton Trans.*, 2015, **44,** 8846-8854. (b) A. Ciupa, M. Mączka, A. Gągor, A. Pikul and M. Ptak, *Dalton Trans.* 2015, **44,** 13234-13241.

37 C. Carabatos-Nedelec and P. Becker, *J. Raman Spectrosc.* 1997, **28,** 663-671.

38 P. Guionneau, M. Marchivie, G. Bravic, J.-F. Letard, D. Chasseau, *Topp. Curr. Chem.* 2004, **234,** 97-128.

39 D.-W. Fu, W. Zhang, H.-L. Cai, J.-Z. Ge, Y. Zhang, R.-G. Xiong, *Adv. Mater.* 2011, **23,** 5658-5662.

40 D.-W. Fu, H.-L. Cai, Y. Liu, Q. Ye, W. Zhang, Y. Zhang, X.-Y. Chen, G. Giovannetti, M. Capone, J. Li, R.-G. Xiong, *Science* 2013, **339,** 425.

Phase I, $P\,2_1/n$ polar Phase II, Pn

468x184mm (96 x 96 DPI)